Analyzing intramolecular dynamics by Fast Lyapunov Indicators

Elena Shchekinova, Cristel Chandre, Yueheng Lan, Turgay Uzer

Analyzing intramolecular dynamics by Fast Lyapunov Indicators

E. Shchekinova[1], C. Chandre[2], Y. Lan[1] and T. Uzer[1]

[1] *Center for Nonlinear Science, School of Physics,*

Georgia Institute of Technology, Atlanta, Georgia 30332-0430, U.S.A.

[2] *Centre de Physique Théorique - CNRS,*

Luminy - Case 907, 13288 Marseille cedex 09, France

Abstract

We report an analysis of intramolecular dynamics of the highly excited planar carbonyl sulfide (OCS) below and at the dissociation threshold by the Fast Lyapunov Indicator (FLI) method. By mapping out the variety of dynamical regimes in the phase space of this molecule, we obtain the degree of regularity of the system versus its energy. We combine this stability analysis with a periodic orbit search, which yields a family of elliptic periodic orbits in the regular part of phase space an a family of in-phase collinear hyperbolic orbits associated with the chaotic regime.

I. INTRODUCTION

Multidimensional, complex systems tend to overwhelm the researcher with data: think of fluid dynamical data from the oceans or the millions of trajectories that today's powerful computers can generate in an instant. In many areas of science and engineering, experimental techniques to observe real-time dynamical phenomena have also developed at a pace far more rapid than the theory required to make sense of such data. In chemistry, a recent example is the rapid development of techniques to study single molecules, such as proteins [1, 2].

For low-dimensional systems, the geometric framework of dynamical systems theory has provided a way of understanding these data. This point of view, first espoused by Poincaré, asks about the relationship between all possible trajectories, rather than the evolution of individual trajectories. This leads immediately to the notion of *phase space structure* as a key notion for making sense of the many and varied regimes that a nonlinear dynamical system can exhibit. However, techniques for mining high-dimensional plethora of data for any underlying structures and geometry have thus far lagged badly behind our ability to generate it.

For Hamiltonian systems with two degrees of freedom, a Poincaré section constructed by a plane section (of dimension 2) of a set of individual trajectories lying on the energy surface of dimension 3 is able to give a clear picture of the dynamics, e.g., of regular versus chaotic regions of phase space. Analyzing the dynamics of higher- dimensional systems by extrapolating this technique is not straightforward since the Poincaré section has dimension 4 for systems with three degrees of freedom. One method to understand high-dimensional systems has been developed by Laskar [3, 4, 5] and relies on visualizing the dynamics in the frequency space. For instance, for three degrees of freedom, this frequency space is of dimension 2 which makes its analysis tractable. It is known as Frequency Map Analysis (FMA) because it is based on extracting the principal frequencies of quasiperiodic trajectories. Clearly, this method is well-suited for nearly integrable systems whose phase space contains many invariant tori. This method has also been extended to weakly chaotic regimes by computing a diffusion coefficient in frequency. The FMA has been first developed in celestial mechanics, and has subsequently been applied in various other fields, like atomic physics [6, 7], particle accelerators [8, 9, 10] and chemistry [11, 12]. For strongly chaotic systems, the notion of frequency and diffusion in frequency are not well defined, so any

Fourier-based analysis like this one must be used with extra caution.

In order to understand the dynamics of high-dimensional systems in the strongly chaotic regime, the computation of Lyapunov exponents based on the linearized flow has been used extensively [13]. However, Lyapunov exponents being infinite-time quantities, the long computational times required for their reliable computation are not suited for an extensive analysis of phase space. Geometrical approaches based on the geodesic deviation equations to study dynamics of many-dimensional continuous dynamical systems have been developed in [14]. Also noteworthy are the investigations of Berry and coworkers concerning the non-uniformity of the dynamical properties of Hamiltonian systems representing atomic clusters with up to 13 atoms. In particular, they explored how regular and chaotic behavior may vary locally with the topography of the potential energy surfaces (PES) [15, 16, 17, 18, 19, 20, 21, 22, 23, 24, 25]. By analyzing local Lyapunov functions and Kolmogorov entropies, they showed that when systems have just enough energy to go through a saddle in the potential energy surface, the system's trajectories become collimated and regularized through the saddle regions, developing approximate local invariants of the motion different from those in the potential well. Recently, numerical methods based on linear stability analysis have been designed to analyze trajectories of Hamiltonian systems, which were obtained by numerical integration of the flow. The aim of these methods is to obtain pictures of the phase space and highlight relevant structures [26, 27, 28]. It has been shown that the relevant information on a typical trajectory is obtained by integrating the flow for a short time. For instance, distinguishing between regular and chaotic trajectories, or even between weakly and strongly chaotic trajectories is possible after a short integration of the equations of motion. The Fast Lyapunov Indicator (FLI) method is one of these highly practical methods.

In this article, we use the FLI method to analyze the internal dynamics of the carbonyl sulfide (OCS) molecule. In its planar and rotationless configuration, this molecule has three coupled modes (two stretching modes and one bending mode). We show how this method helps to visualize the dynamics of highly excited molecules without resorting to dimensional reduction schemes with their attendant flaws and loss of information. In particular, the Fast Lyapunov Indicator method shows global pictures of the dynamics, highlighting regular and chaotic zones. We combine the analysis of the dynamics of OCS with a determination of the main periodic orbits. Our numerical investigations yield the following picture : The regular region is located in the center of the configuration space and is characterized by a family of

elliptic periodic orbits. The strongly chaotic region is entered when the CS stretching mode is highly excited and this region is characterized by a set of collinear hyperbolic periodic orbits which have an additional property of being 'in-phase' (meaning that the bending mode is frozen and the two stretching modes are vibrating with the same frequency).

In Sec. II, we briefly give the explicit expression of the flow of the OCS. In Sec. III, we explain the basics of the Lyapunov indicator method. The numerical results are given in Sec. IV.

II. THE MODEL

The classical model of the planar (rotationless) carbonyl sulfide OCS molecule has been studied in details in Refs. [29, 30, 31, 32, 33, 34]. The coordinates of this system are two interatomic distances $R_1 = d(C,S)$, $R_2 = d(C,O)$, the bending angle of the molecule $\alpha = \widehat{OCS}$, and three momenta P_1, P_2, P_α which are conjugate to R_1, R_2 and α, respectively . We note that the third interatomic distance $R_3 = d(O,S)$ is expressible as a function of R_1, R_2 and α :

$$R_3 = \left(R_1^2 + R_2^2 - 2R_1R_2\cos\alpha\right)^{1/2}.$$

The Hamiltonian for this system is

$$H(R_1,R_2,\alpha,P_1,P_2,P_\alpha) = T(R_1,R_2,\alpha,P_1,P_2,P_\alpha) + V(R_1,R_2,\alpha), \tag{1}$$

where T is the kinetic part of the Hamiltonian and V is the potential. The kinetic part has the form [35]

$$\begin{aligned} T \;=\; & \frac{\mu_1}{2}P_1^2 + \frac{\mu_2}{2}P_2^2 + \mu_3 P_1 P_2\cos\alpha \\ & + P_\alpha^2\left(\frac{\mu_1}{2R_1^2} + \frac{\mu_2}{2R_2^2} - \frac{\mu_3\cos\alpha}{R_1R_2}\right) - \mu_3 P_\alpha \sin\alpha\left(\frac{P_1}{R_2} + \frac{P_2}{R_1}\right), \end{aligned}$$

where μ_i are the reduced masses. The analytic expression of the potential has been proposed based on existing experimental data [36] and can be summarized as :

$$V(R_1,R_2,\alpha) = \sum_{i=1}^{3} V_i(R_i) + V_I(R_1,R_2,R_3), \tag{2}$$

where V_i are Morse potentials for each diatomic pair

$$V_i(R) = D_i\left(1 - e^{-\beta_i(R-R_i^*)}\right)^2,$$

and V_I is the interaction potential of the Sorbie-Murrell form given in Ref. [29] :

$$V_I = P(R_1, R_2, R_3) \prod_{i=1}^{3} \left(1 - \tanh \gamma_i (R_i - R_i^{(0)})\right),$$

where $R_i^{(0)}$ are the equilibrium distances of the planar OCS which is a collinear ($\alpha = \pi$) configuration : $R_1^{(0)} = 2.9508$ (in atomic units) $R_2^{(0)} = 2.2030$ and $R_3^{(0)} = R_1^{(0)} + R_2^{(0)}$. The function P is a quartic polynomial in each of its variables. All the coefficients of the potential are provided in Ref. [29].

The planar OCS is an example of a general triatomic molecule with three strongly coupled modes : OC and CS stretching modes, represented by $R_1(t)$ and $R_2(t)$ and a bending mode, represented by $\alpha(t)$. Any perturbation introduced into one of the modes will be redistributed among the two other modes. It was shown in Ref. [29] that the dynamics of the system is highly irregular at the energies close to the dissociation threshold, which occurs at $E = 0.1$ (in atomic units).

III. THE FAST LYAPUNOV INDICATOR METHOD

The Fast Lyapunov Indicator (FLI) method was introduced in Ref. [37] and rigorous results can be found for the case of near integrable systems in Ref. [26]. The method is similar to the computation of finite time Lyapunov exponents [38]. Given a d-dimensional flow

$$\frac{d\mathbf{x}}{dt} = \mathbf{f}(\mathbf{x}),$$

we are looking at the evolution of a vector $\mathbf{v}$ which is given by the tangent flow

$$\frac{d\mathbf{v}}{dt} = Df(\mathbf{x}) \cdot \mathbf{v},$$

where Df is the matrix of the variations of the flow given by the velocity field $\mathbf{f}$, i.e. $[Df]_{ij} = \partial f_i / \partial x_j$. We integrate the above system of equations starting with initial conditions $\mathbf{x}_0$ and $\mathbf{v}_0$. In principle, one should consider the dynamics of the $d \times d$ Jacobian matrix $J(t)$ which is given by

$$\frac{dJ}{dt} = Df(\mathbf{x})J,$$

(where $J(0)$ is the $d \times d$ identity matrix), in order to study the stability of a given trajectory [39]. The evolution of $\mathbf{v}$ is thus given by $\mathbf{v}(t) = J(t)\mathbf{v}_0$. However, for practical purposes,

we only integrate the equations for $\mathbf{v}(t)$ starting with a given $\mathbf{v}_0$ fixed once and for all. We will omit the dependence on $\mathbf{v}_0$ which will be a valid assumption for large time since most of the vectors $\mathbf{v}_0$ will follow the dynamics of the most unstable eigenvector of $J(t)$.
The Lyapunov indicator is based on the computation of the dynamical variable $\phi(t)$ which is defined as follows:

$$\phi(t;\mathbf{x}_0) = \max_{0\leq t'\leq t} \log \|\mathbf{v}(t';\mathbf{x}_0)\|, \tag{3}$$

where $\mathbf{v}(t;\mathbf{x}_0)$ is a tangent vector of the flow at time t for the trajectory starting with initial conditions $\mathbf{x}_0$. The Lyapunov indicator $\phi(t;\mathbf{x}_0)$ is a monotonically increasing function of time. Not only can it distinguish regular from chaotic motion but is also an indicator of resonant and nonresonant trajectories for nearly integrable systems [26].

For instance, a chaotic trajectory is characterized by an exponential separation of nearby trajectories. The resulting Lyapunov indicator grows linearly in time (the coefficient of this growth will be asymptotically the largest Lyapunov exponent). In the regular region, a good model is provided by considering an integrable Hamiltonian with action-angle coordinates $(\mathbf{A},\boldsymbol{\varphi}) \in \mathbb{R}^d \times \mathbb{T}^d$ where $\mathbb{T}^d$ is the d-dimensional torus. The Hamiltonian writes $H_0 = H_0(\mathbf{A})$ and the equations of motion are the following ones

$$\begin{aligned} \frac{d\mathbf{A}}{dt} &= \mathbf{0}, \\ \frac{d\boldsymbol{\varphi}}{dt} &= \frac{\partial H_0}{\partial \mathbf{A}} = \boldsymbol{\omega}(\mathbf{A}). \end{aligned}$$

The tangent flow is given by

$$\frac{d\mathbf{v}}{dt} = \begin{pmatrix} 0 & 0 \\ \boldsymbol{\omega}'(\mathbf{A}) & 0 \end{pmatrix} \cdot \mathbf{v},$$

where $\boldsymbol{\omega}'(\mathbf{A})$ is a $d \times d$ matrix whose elements are $\partial\omega_i/\partial A_j$. Since $\mathbf{A}$ is constant along a trajectory, the evolution of the vector $\mathbf{v}$ is linear in time. Therefore, the Lyapunov indicator evolves like

$$\phi(t) \approx \log t.$$

More precise results are obtained in the nearly integrable regime [26]. There is a linear growth in the chaotic region and a logarithmic growth in the regular region. For t large enough, the Fast Lyapunov indicator makes a clear distinction between regular and chaotic trajectories as we will show numerically for the OCS molecule. Our numerical observation is that this indicator achieves this distinction very early in time compared with other existing methods.

The maps of the dynamics are obtained by examining the values of this Lyapunov indicator at a fixed time as a function of initial conditions.

$$\mathbf{x}_0 \mapsto \phi(t; \mathbf{x}_0).$$

In spirit, this method is very similar to Frequency Map Analysis [5, 40] where instead of a Lyapunov indicator, a diffusion in frequency is plotted as function of the initial conditions. The main feature of the FLI method is that it reveals the important phase space structures which makes the method an appropriate tool for the investigation of the classical phase space of highly excited molecules.

IV. NUMERICAL RESULTS

We investigated the phase space structures including existing resonances and periodic trajectories and analyzed the stability properties for different regions in the configuration space of OCS.

In what follows we consider trajectories with initial conditions in the configuration space (R_1, R_2), i.e. we consider initially that $P_1 = P_2 = P_\alpha = 0$ and the initial value of the angle α is determined by the energy integral $V(R_1, R_2, \alpha) = E$. The FLI as a function of time is computed in the time interval $t \in [0, 1]$ (the unit of time is one picosecond), which is long enough for the system to show the characteristic dynamics. The integration of the equations of motion is carried out using a standard variable order Adams-Bashforth-Moulton PECE solver. Figure 1 depicts the variations of the Lyapunov indicator ϕ as a function of time for four distinct trajectories at an energy $E = 0.09$ (in atomic units, where the value of the energy is given with respect to the equilibrium energy) : one periodic, one quasiperiodic, one weakly chaotic and one strongly chaotic orbit. A projection on the plane (R_1, R_2) of each of these four trajectories computed for $t \in [0, 1]$ is depicted on Fig. 2. These figures show the power of the Fast Lyapunov indicator: Not only can it distinguish between regular and chaotic trajectories but also between resonant and non-resonant regular trajectories and between weakly and strongly chaotic trajectories. To set the scale, this distinction is made as early as at time $t = 1$. As a comparison, the molecule has a period of 0.063 in the periodic case (the periodic orbit O_a, see below), i.e. $t = 1$ corresponds to about 15 periods of oscillation of the molecule.

Fields of Fast Lyapunov Indicators were computed on an equally spaced grid of initial conditions in the configuration space (R_1, R_2) for different energies. The computations for the FLI are carried out on the time interval $t \in [0, 1]$. For each initial condition (R_1, R_2), the maximum value attained by FLI during the time interval $[0, 1]$ ps is plotted. The result is the Lyapunov field for a given value of the energy. Figure 3 depicts the Lyapunov field for $E = 0.09$. The dark regions of this Lyapunov field are associated with regular regions and the white regions with chaotic trajectories.

In order to check these results, we computed the main periodic orbits and their stability at this energy. We found these periodic orbits by a novel variational method which provides a very robust determination of periodic orbits of flows [41, 42]. This method can determine periodic orbits of flows regardless of their stability properties (elliptic or hyperbolic periodic orbits). A brief description follows.
We start from a point in the configuration subspace and evolve it for some time. We take $R_1 = 3$ to be our Poincaré section by noticing that most of the time the orbit intersects this hyperplane. The flow becomes a map on the Poincaré section. As the symbolic dynamics of this system is yet unexplored, to obtain cycles of different topological length, we look for the near-recurrence of the map on the section for one iteration, two iterations, three iterations, etc. The resulting orbit segment is represented by a discrete set of points and its frequency components are obtained by a Fast Fourier Transform. After removing the high-frequency part, we transform the data back to the phase space and obtain a closed smooth loop, which becomes our starting guess for a periodic orbit. A Newton descent flow will drive the orbit toward a genuine periodic orbit by penalizing the discrepancy between the approximate flow and the true flow along the loop [41, 42]. Table I lists all the elliptic periodic orbits we have obtained using this method : Two projections of each periodic orbit are given, one on the plane (R_1, P_1) and the other on the plane (R_2, P_2). The period T is also given in picosecond as well as the value of the resonance $m : n : k$. These integers are computed using the following procedure : We compute by frequency analysis the main frequencies ω_1, ω_2 and ω_3 of the three signals, respectively, $z_1(t) = R_1 + iP_1$, $z_2(t) = R_2 + iP_2$ and $z_3 = \alpha + iP_\alpha$. The integers m, n, k are such that $\omega_1/\omega_2 = m/n$, $\omega_2/\omega_3 = n/k$. Each of these periodic orbits intersects the configuration space at two different points. These points are represented on Fig. 3. Our main observation is that the center of the configuration space is weakly chaotic

and characterized by two elliptic periodic orbits O_a and O_b.

We have also computed the main hyperbolic periodic orbits of OCS. The intersection of these periodic orbits with the configuration space is plotted on Fig. 3. We notice that the boundary of the configuration space which mostly chaotic is characterized by hyperbolic periodic orbits. Moreover, by frequency analysis we show that these hyperbolic periodic orbits are collinear ones, i.e., the bending mode is frozen and the stretching modes are in-phase ($1:1:0$ resonances).

We note that the chaotic trajectories appear when R_1 is large or R_1 is small. Therefore the stretching mode CS appears to lead the dynamics of the molecule. Moreover since in-phase collinear hyperbolic periodic orbits appear when R_1 is large, these type of periodic orbits are likely to lead the chaotic behavior near the dissociation threshold.

The resulting data on FLI values for all the initial conditions corresponding to the different dynamical regimes allow one to introduce a classification of the orbits and to compute the percentage of the regular and irregular orbits for the system for different values of the energy and to compare those results with an existing classification. In Ref. [29] the classification was done by using the behavior of the Lyapunov exponents for microcanonically chosen trajectories at different energies. Here, we examine the evolution of FLI curves for different initial conditions in the configuration space. As a result the threshold value of the FLI can be introduced for filtering regular and irregular motions. We have noticed that for the majority of trajectories studied the motion is chaotic or weakly chaotic above the value $\phi_c = 10$ (which is evaluated at $t = 1$).

Figure 4 depicts the Lyapunov fields for six different values of the energy, from $E = 0.05$ up to the dissociation energy $E = 0.1$. One can observe the evolution of the global stability of the system as the energy is increased. Dark regions correspond to low values of FLI, that is to say, to regular regions, whereas light regions are associated with high values of the FLI where chaotic trajectories are predominant. The color scale is chosen to be the same for each energy in order to observe in a clearer way the changes in phase space as energy increases. The FLI field for the energy $E = 0.05$ consists of a dark region in the center associated with a set of elliptic periodic and quasiperiodic orbits with frequency ratios $\omega_1/\omega_\alpha = 2,\ \omega_2/\omega_\alpha = 2$ where ω_1, ω_2 and ω_α are the main frequencies of the signals $R_1(t) + iP_1(t),\ R_2(t) + iP_2(t)$ and $\alpha(t) + iP_\alpha(t)$, respectively. Smaller dark regions are associated with higher order resonances. Most of trajectories are quasiperiodic for this

energy since the values of the FLI $\phi(t=1)$ are smaller than ϕ_c. As the energy is increased to $E = 0.0639$ some regular motions lose stability and chaotic motions appear. They can be seen in the lower left corner of the configuration space (R_1, R_2). Highlighted ridges spiraling around the central resonance region are associated with hyperbolic periodic trajectories. They separate the main resonant zone with the frequency ratios $\omega_1/\omega_\alpha = 2,\ \omega_2/\omega_\alpha = 2$ from other higher order resonant zones. We notice that the FLI fields do not provide a precise determination of the locations of hyperbolic periodic orbits because its resolution is not sharp enough and some regions do overlap. For the energies $E = 0.07$ and $E = 0.08$ more chaotic trajectories appear and the overall dynamics is more chaotic. This is indicated by the increasing number of points with higher values of the FLI (the value of FLI reaches 22 for the $E = 0.08$) in the configuration space. We notice that at $E = 0.07$ a bifurcation of the main resonance $2:2:1$ has occurred. The central island which leads the regular dynamics for $E < 0.07$ is split into two parts. These regular parts are connected and survive for larger energies, even near the dissociation threshold. They are associated with a resonance $1:4:1$. For the energy $E = 0.098$, only a few regular regions around elliptic periodic orbits remain. They are separated by a large set of initial conditions corresponding to chaotic motions. We identify all the surviving resonances by computing the frequency ratios for the trajectories generated inside the islands.

For energies close to dissociation (see for instance Fig. $1(f)$), most of the Lyapunov field consists of initial conditions associated with strongly chaotic motions : The values of the FLI $\phi(t=1)$ are larger than 16 except several resonant islands and the percentage of regular behavior is below 30%. These remaining islands correspond to elliptic periodic orbits. Large dark zones appear on th right hand side of the FLI fields for $R_1 > 4.8$. In order to get insight into the presence of low values of the FLI for initial conditions in regions where we expect a priori strongly chaotic motions, the time sequences for R_1 and R_2 and the evolution of the FLI are plotted on Figs. 5 and 6 for two typical trajectories with initial conditions such that $R_1 > 4.75$. Here the FLI is defined as $\phi(t) = \log \|v(t)\|$ for convenience. We observe that for the trajectory corresponding to the dissociation of the molecule (see Fig. 5) the value of the FLI grows slowly (logarithmically). This is due to the fact that C and O atoms are moving under the influence of Morse potential V_2 mostly. Contributions from the other terms in the potential are too small to affect the dynamics. The system is very close to integrability. For the trajectory near the dissociation (see Fig. 6) we observe an intermittent

behavior in the time sequence for the R_2. Regular oscillations are interrupted by higher amplitude peaks. Regular motion corresponds to the intervals of time when the S atom is far from the CO bond to affect the dynamics. During this interval of time the quantity of the FLI is decreasing. This has a significant effect on the resulting largest value of FLI at the end of the interval of time. From the FLI fields, we observe that the region with high values of the FLI is sharply joint at $R_1 \in [4.7, 4.8]$ with the region where trajectories dissociate or demonstrate an intermittent behaviour discussed above. At this stage, it is not clear whether there is a surface barrier dividing phase space into twoparts with completely distinct dynamics and what the conditions are on an initial configuration of the OCS for the trajectories to show one or the other type of dynamical behaviour.

We use the FLI field data to compute the percentage of regular versus irregular orbits for the system at different energies. We compare our results with an existing classification in Ref. [29]. The percentage of regular motions for different values of the energy E is plotted versus E on Fig. 7. Our computations give the bounds for the critical energy for the onset of irregularities in the system which are $0.05 < E_c < 0.0639$. This result agrees with the value for the critical energy $E = 0.0639$ calculated in Ref. [29]. However at the energy close to dissociation ($E = 0.098$), we observe many more regular trajectories than the estimate given in Ref. [29]. This can be due to the fact that in our studies we calculated FLI for 132×110 trajectories whereas the previous stability analysis was performed for 20 microcanonically distributed trajectories in Ref. [29], and also to the fact that we consider initial trajectories in the configuration space (i.e. with zero kinetic energy). For the interval of energy $0.07 < E < 0.08$ we see a significant change in the dynamical behavior of the system. About 15% of regular trajectories lose their stability. Therefore most of the important bifurcations in this system happen in this interval of energy.

Conclusions

We have applied the Fast Lyapunov Indicator method in the phase space of highly excited planar OCS. This method is based on an analysis of the linear stability of trajectories. It gives pictures of the dynamical regimes in phase space, analogous to Poincaré sections for systems with two degrees of freedom. In conjunction with a search of periodic orbits, this method gives insights into the dynamics of intramolecular energy flow in highly excited

molecules. We have applied this method to planar OCS with energies below and at the dissociation threshold. The main results are as follows: When the energy is well-distributed among the three modes in the center of the configuration space, the behavior is regular. When the bending mode is frozen and the two stretching modes are in phase (O and S are vibrating in opposite phase) chaotic behavior is seen. We have provided pictures of phase space for different values of the energy below and at the dissociation threshold : It allows one to identify the mechanism of transition to chaos and dissociation.

---

[1] H.P. Lu, L. Xun, and X.S. Xie, Science **282**, 1 (1998).

[2] J.N. Onuchic, J. Wang, and P. Wolynes, Chem. Phys. **247**, 175 (1999).

[3] J. Laskar, Icarus **88**, 266 (1990).

[4] J. Laskar, Physica D **67**, 257 (1993).

[5] J. Laskar, in *Hamiltonian Systems with Three or More Degrees of Freedom*, *NATO ASI Series*, edited by C. Simó (Kluwer Academic Publishers, Dordrecht, 1999), p. 134.

[6] J. von Milczewski, G.H.F. Diercksen and T. Uzer, Phys. Rev. Lett. **76**, 2890 (1996).

[7] J. von Milczewski, D. Farrelly and T. Uzer, Phys. Rev. Lett. **78**, 1436 (1997).

[8] S. Dumas and J. Laskar, Phys. Rev. Lett. **70**, 2975 (1993).

[9] J. Laskar and D. Robin, Particle Accelerator **54** 183 (1996).

[10] D. Robin, C. Steier, J. Laskar and L.S. Nadolski, Phys. Rev. Lett. **85**, 558 (2000).

[11] J.C. Losada, J.M. Estebaranz, R.M. Benito and F. Borondo, J. Chem. Phys. **108**, 63 (1998).

[12] J. von Milczewski and T. Uzer. Mapping multidimensional intramolecular dynamics using frequency analysis. In D.L. Thompson, editor, *Modern Methods for Multidimensional Dynamics Computations in Chemistry*, pages 190 – 200, Singapore, 1998. World Scientific.

[13] A.J. Lichtenberg and M.A. Lieberman, *Regular and Stochastic Motion*, (Springer-Verlag, New-York, 1983).

[14] P. Cipriani, M. Bari, Planet. Space Science **46**, 1543 (1998).

[15] T.L. Beck, D.M. Leither and R.S. Berry, J. Chem. Phys. **89**, 1681 (1998).

[16] D.J. Wales and R.S. Berry, J. Physics B **24**, L351 (1991).

[17] R.J. Hinde, R.S. Berry and D.J. Wales, J. Chem. Phys. **96**, 1376 (1992).

[18] C. Amitrano and R.S. Berry, Phys. Rev. Lett. **68**, 729 (1992).

[19] C. Amitrano and R.S. Berry, Phys. Rev. E **47**, 3158 (1993).

[20] R.S. Berry, Chem. Rev. **93**, 237 (1993).

[21] R.J. Hinde and R.S. Berry, J. Chem. Phys. **99**, 2942 (1993).

[22] R.S. Berry, Int. J. Quantum Chem. **58**, 657 (1996).

[23] S.K. Nayak, P. Jena, K.D. Ball and R.S. Berry, J. Chem. Phys. **108**, 234 (1998).

[24] T. Komatsuzaki and R.S. Berry, J. Chem. Phys. **110**, 9160 (1999).

[25] T. Komatsuzaki and R.S. Berry, Adv. Chem. Phys. **123**, 79 (2002).

[26] M. Guzzo, E. Lega, C. Froeschlé, Physica D **163**, 1 (2002).

[27] P.M. Cincotta and C. Simó, Astron. Astrophys. Sup. **147**, 205 (2000).

[28] P.M. Cincotta, C.M. Giordano and C. Simó, Physica D **182**, 151 (2003).

[29] D. Carter, P. Brumer, J. Chem. Phys. **77**, 4208 (1982); J. Chem. Phys. **78** (erratum), 2104 (1983).

[30] M.J. Davis, Chem. Phys. Lett. **110**, 491 (1984).

[31] M.J. Davis and A.F. Wagner, in *Resonances in Electron-Molecule Scattering, van der Waals Complexes, and Reactive Chemical Dynamics*, edited by D. G. Truhlar (American Chemical Society Symposium Series No. 263, Washington,1984).

[32] M.J. Davis, J. Chem. Phys. **83**, 1016 (1985).

[33] C.C. Martens, M.J. Davis, and G.S. Ezra, Chem. Phys. Lett. **142**, 519 (1987).

[34] C.C. Martens, PhD thesis, Cornell University, 1987.

[35] D.L. Bunker, J. Chem. Phys. **37**, 393 (1962).

[36] A. Foord, J.G. Smith and D.H. Whiffen, Mol. Phys. **29**, 1685 (1975).

[37] C. Froeschlé, E. Lega, R. Gonczi, Celest. Mech. Dyn. Astron. **67**, 41 (1997).

[38] T. Okushima, Phys. Rev. Lett. **91**, 254101 (2003).

[39] P. Cvitanović, R. Artuso, R. Mainieri, G. Tanner and G. Vattay, *Chaos: Classical and Quantum*, `www.nbi.dk/ChaosBook/` (Niels Bohr Institute, Copenhagen 2003).

[40] J. Laskar, C. Froeschlé, and A. Celletti, Physica D **56**,253 (1992).

[41] P. Cvitanović and Y. Lan, in *Proceed. of 10. Intern. Workshop on Multiparticle Production: Correlations and Fluctuations in QCD* edited by N. Antoniou, (World Scientific, Singapore 2003).

[42] Y. Lan and P. Cvitanović, to appear in Phys. Rev. E (2004).

FIGURES CAPTIONS

Figure 1.

FLI versus time curves for the OCS system for the initial conditions for chaotic, weakly chaotic, quasiperiodic and periodic orbits respectively: a) ($2.762, 1.911$), b) ($3.67, 2.307595$), c) ($3.65, 2.307595$), d) ($3.615178, 2.307595$).

Figure 2.

Trajectories in the configuration space for the three initial conditions of Fig. 1. Trajectories (b) and (c) are chosen in the vicinity of the periodic orbit O_a which is represented by the trajectory (d). The time of integration is 1ps.

Figure 3.

Contour plot for the FLI values in the configuration space (R_1, R_2) of the OCS molecule for $E = 0.09$. The circles represent elliptic periodic orbits and crosses represent collinear hyperbolic periodic orbits.

Figure 4

Contour plots for the FLI values in the configuration space (R_1, R_2) of the OCS molecule given at the energies: a) $E = 0.05$, b) $E = 0.0639$, c) $E = 0.07$, d) $E = 0.08$, e) $E = 0.098$, f) $E = 0.1$.

Figure 5

Time series of R_1, R_2 and the FLI evolution for the trajectory at the dissociation energy $E = 0.1$. Initial condition : $R_1 = 4.8$, $R_2 = 2.145$.

Figure 6

Time series of R_1, R_2 and the FLI evolution for the trajectory near the dissociation energy. Initial condition : $R_1 = 5.02$, $R_2 = 2.11$.

Figure 7

Percent of regular trajectories versus energy for the OCS. The interval of energy is E $\in$ [$0.05, 0.098$].

Name	Projection (R_1, P_1) and (R_2, P_2)	T (ps)	(R_1, R_2)	$m : n : k$
O_a	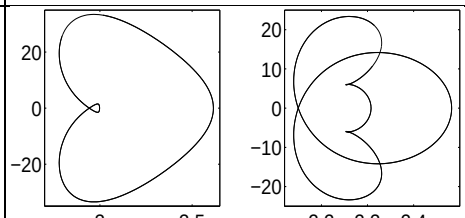	0.063	(3.615178, 2.307595) (2.998235, 2.482408)	1 : 1 : 1
O_b	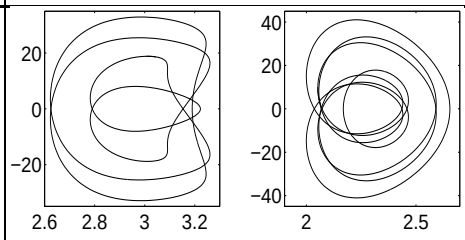	0.122	(3.189711, 2.654841) (3.222491, 2.168308)	2 : 3 : 1
O_c	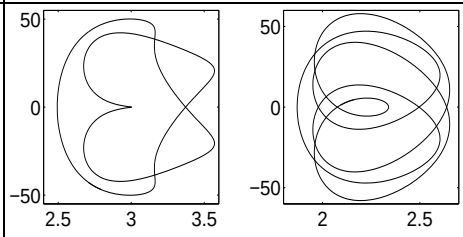	0.087	(2.493375, 2.339454) (3.002806, 1.869968)	2 : 2 : 1
O_d	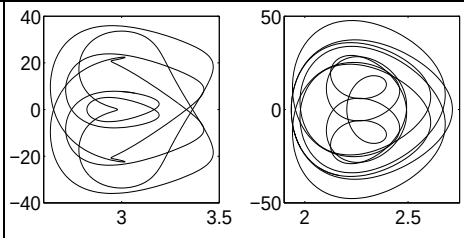	0.195	(2.821580, 2.714920) (2.978729, 2.203665)	4 : 11 : 3
O_e	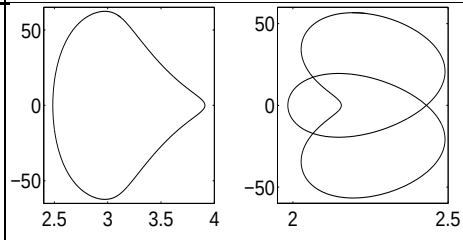	0.049	(3.911413, 1.983623) (2.485514, 2.155984)	1 : 1 : 0

TABLE I: Characteristics of the main elliptic periodic orbits : two projections on the planes (R_1, P_1) and (R_2, P_2) are given. We also provide the period T expressed in picoseconds and the two points which are the intersections of the orbits with the configuration space.

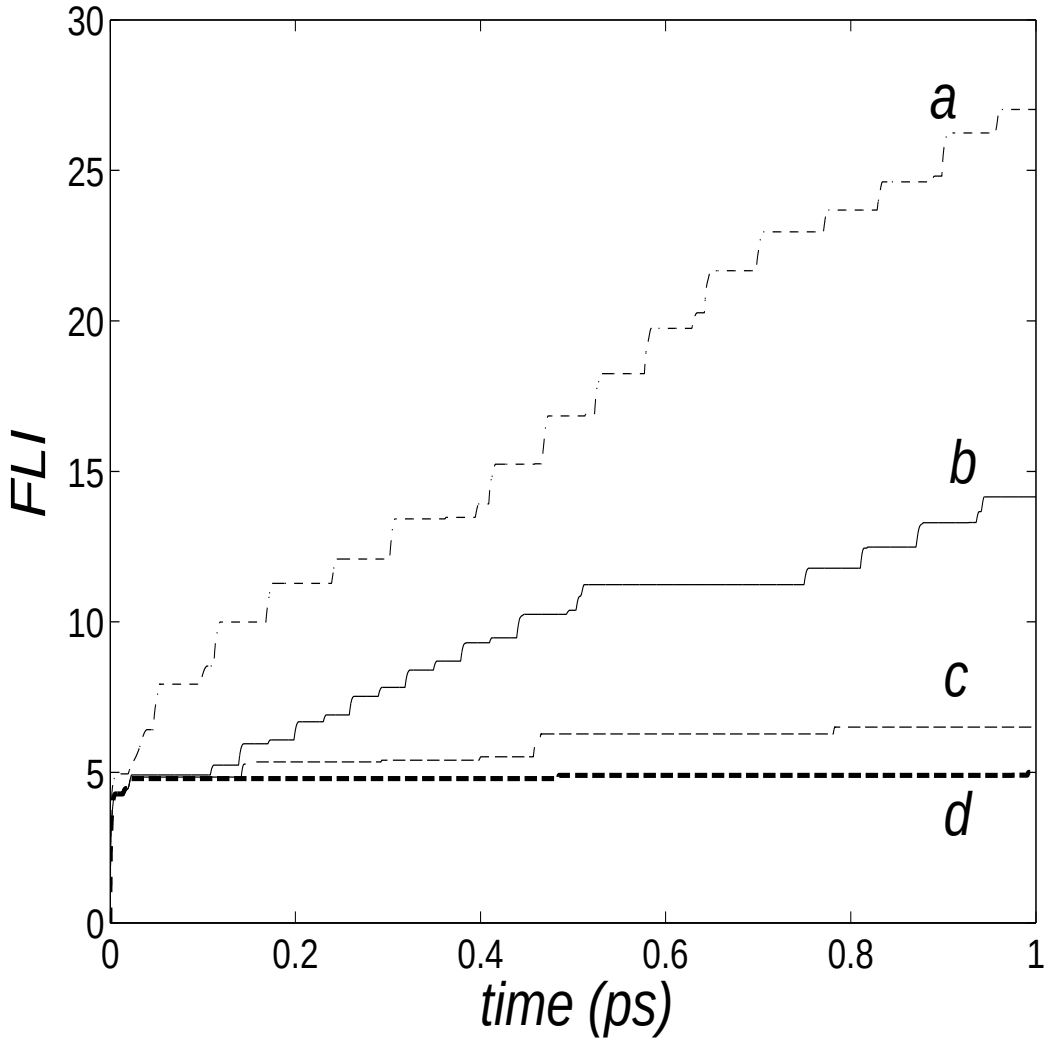

FIG. 1:

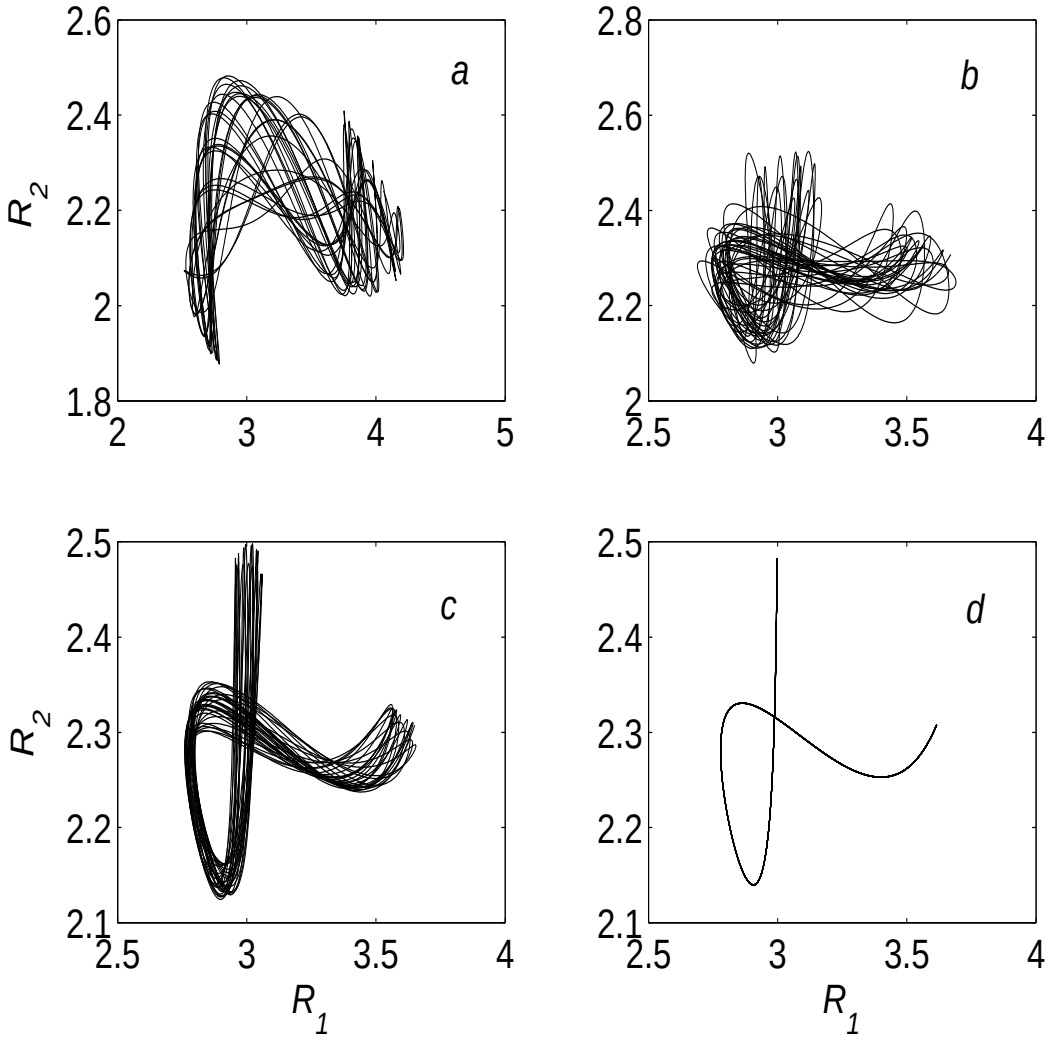
a
b
c
d
R_2
R_1
2.6
2.4
2.2
2
1.8
2
3
4
5
2.8
2.6
2.4
2.2
2
2.5
3
3.5
4
2.5
2.4
2.3
2.2
2.1
2.5
3
3.5
4

FIG. 2:

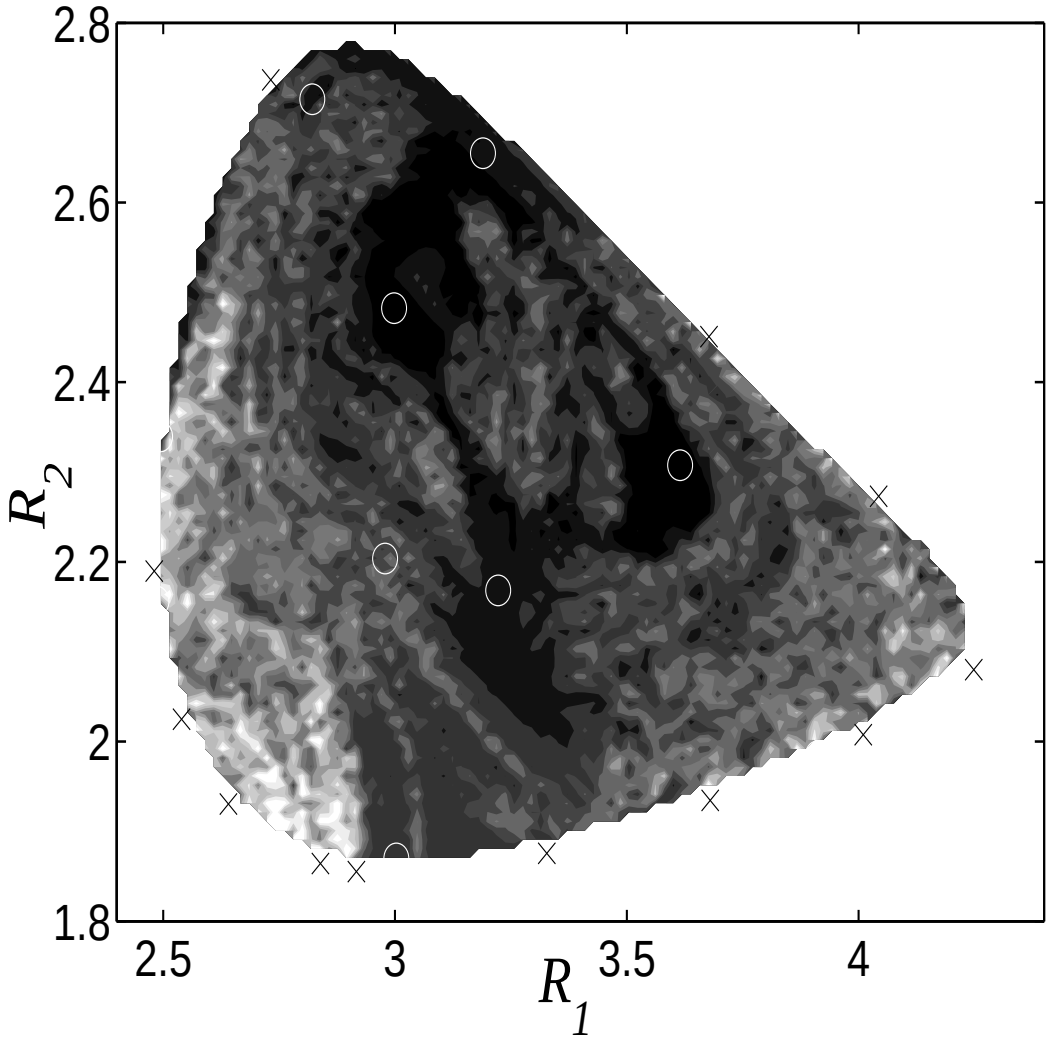

FIG. 3:

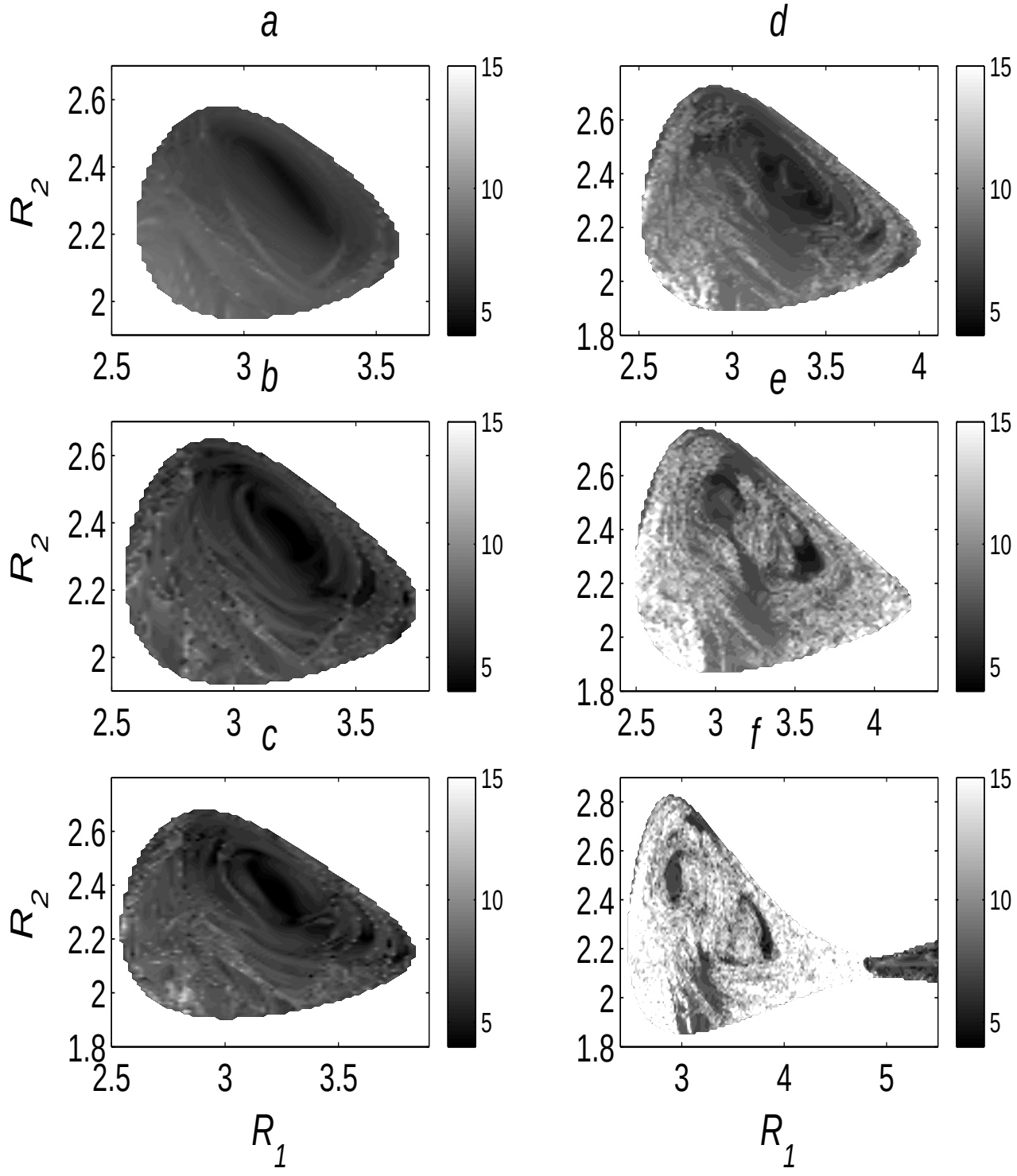

FIG. 4:

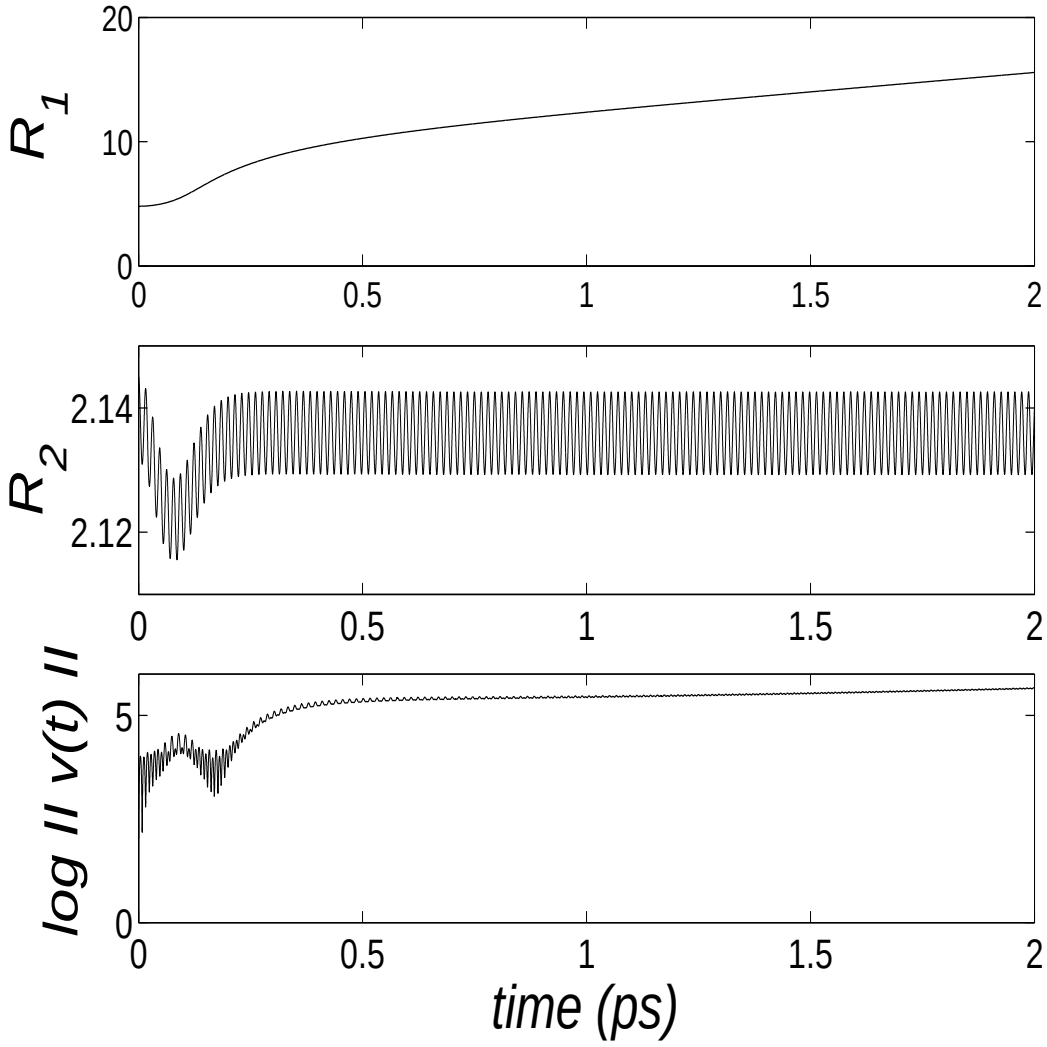
20
10
0
R_1
0
0.5
1
1.5
2
2.14
2.12
R_2
0
0.5
1
1.5
2
5
0
log II v(t) II
0
0.5
1
1.5
2
time (ps)

FIG. 5:

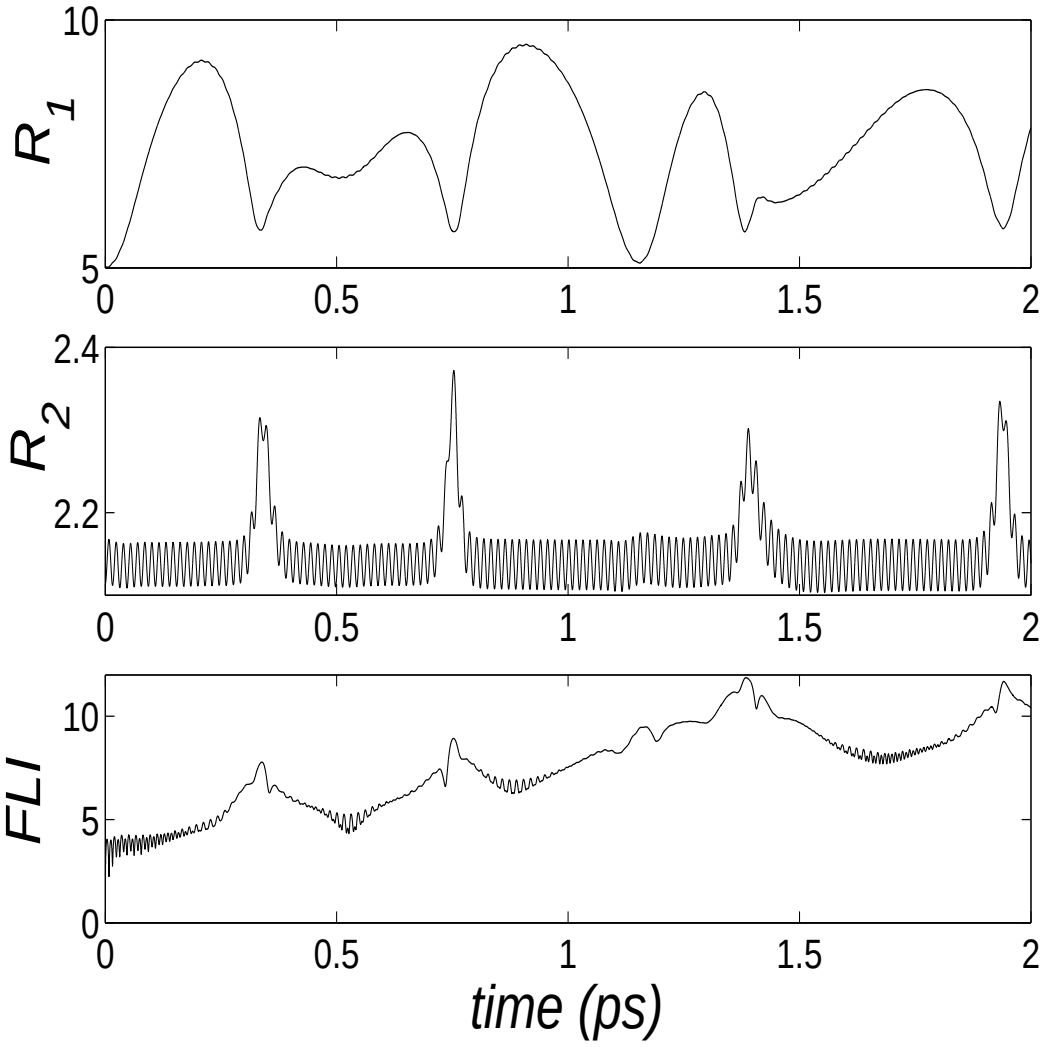

FIG. 6:

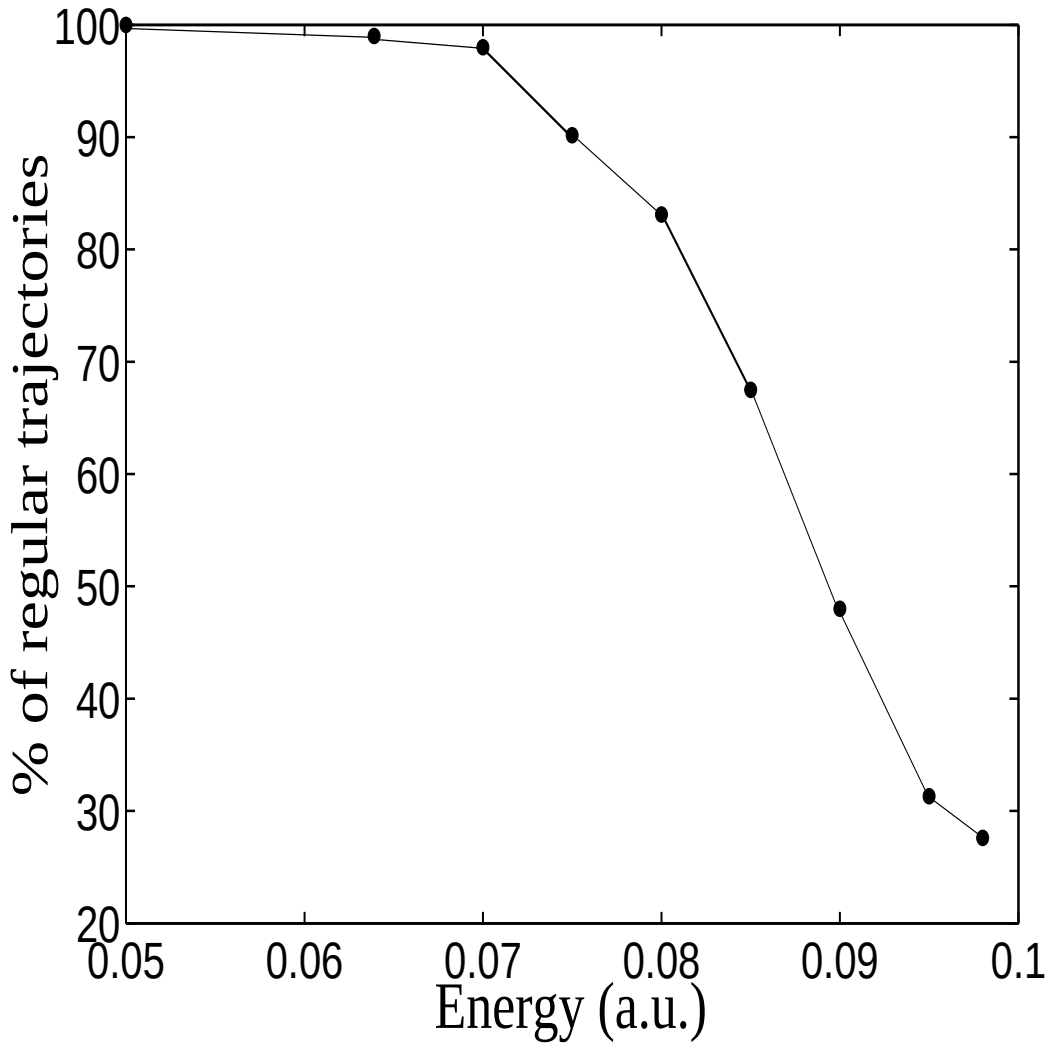
100
90
80
70
60
50
40
30
20
% of regular trajectories
0.05
0.06
0.07
0.08
0.09
0.1
Energy (a.u.)

FIG. 7: